Data Assimilation in a Simple Tropical Ocean Model with Wind Stress Errors

ZHENG HAO AND MICHAEL GHIL*

Climate Dynamics Center and Department of Atmospheric Sciences, University of California at Los Angeles, Los Angeles, California

(Manuscript received 1 June 1992, in final form 2 February 1994)

ABSTRACT

A major error source in the numerical simulation of tropical oceans is the uncertainty in wind stress forcing. A reduced-gravity shallow-water model has been used to test how assimilated ocean data correct simulation errors caused by erroneous wind stress in the tropics. The geometry of the basin is rectangular and symmetric about the equator, and the long-wave approximation is applied. All experiments are of the identical-twin type: the "observations" are generated by sampling the desired reference solution, and the data are assimilated by optimal interpolation into the same model, with wind stress forcing different from that in the reference case.

In this paper, three types of wind stress errors are considered: errors of timing only, as well as persistent errors, systematic or stochastic. The relative usefulness of thermocline depth and current observations, and the effect of data distribution on state estimation are examined. The role of equatorial ocean waves in the process of data assimilation is also studied.

1. Introduction

Tropical ocean circulation plays an important role in the global climate. Recent simulations of the seasonal cycle and the El Niño phenomenon using ocean models forced with observed wind stress fields exhibit considerable verisimilitude, whether the models were relatively simple or more elaborate (e.g., Busalacchi and O'Brien 1981; Cane and Zebiak 1985; Philander et al. 1987a). These results suggest that the tropical ocean is largely a forced system, with little internal variability on seasonal and interannual timescales. Given good knowledge of surface forcing—surface fluxes of momentum, heat, and freshwater—and a perfect model, it seems that one can simulate the low-frequency variability of the tropical ocean. However, since ocean models are not perfect and the surface forcing is poorly known, measurements of the ocean state are needed to correct model errors, for both simulation and prediction.

Extensive experience with data assimilation has been gained from its operational application in numerical weather prediction (NWP). Still, data assimilation in a tropical ocean model differs from NWP. A major factor that limits the predictability of an atmospheric model is errors in the initial state. As NWP concentrates on timescales of hours to days, the inertia–gravity waves excited by imbalance in the initial state can affect negatively the assimilation cycle (Baer 1977; Daley 1981). However, the timescales considered in tropical ocean simulations are longer than a month, and over such long timescales, the inertia–gravity waves due to initial imbalance dissipate and become unimportant.

Physical instabilities with a timescale of about a month are associated with the meridional shear of the significant zonal currents near the equator but do not cascade energy to lower frequencies (Philander et al. 1985). No other low-frequency instabilities are known for the tropical ocean by itself, without coupling to the atmosphere. Hence, amplification of errors in initial data is not as important as it is in the atmosphere for simulations of seasonal and interannual variability in the tropical ocean (Philander et al. 1987b).

Two factors that substantially restrict the simulation and prediction capabilities of tropical ocean models are poorly known surface fluxes and the ad hoc parameterization of physical processes. Defects in the parameterization of mixing processes cause the sharp, shallow tropical thermocline to diffuse downward, thus changing the thermal field, especially the sea surface temperatures. In one-layer reduced-gravity shallow-water models, this is not a problem because the existence of the thermocline is taken for granted and only changes in vertical position of the specified thermocline are simulated.

Uncertainties in the surface stress field generate differences in sea surface temperature and subsurface thermal structure that are comparable with the observed seasonal and interannual variability of the tropical Pacific Ocean (Leetmaa and Ji 1989). Thus, the

* Additional affiliation: Institute of Geophysics and Planetary Physics, University of California at Los Angeles, Los Angeles, California.

Corresponding author address: Dr. Michael Ghil, Dept. of Atmospheric Sciences, 405 Hilgard Ave., University of California at Los Angeles, Los Angeles, CA 90024-1565.

role of data assimilation in tropical ocean models is not only to correct errors in initial data but, also and more importantly, to correct errors caused by the model parameterization and the surface flux deficiencies.

The main questions for data assimilation in general are (i) how different variables determine the state of the system and (ii) how the observed information propagates within the system (Ghil and Malanotte-Rizzoli 1991). The propagation of information from data localized in space to other regions of the ocean has been addressed in tropical oceanography by Moore et al. (1987), Miller and Cane (1989), Moore and Anderson (1989), and Smedstad (1989). Their results suggest that equatorially trapped waves dominate the information transfer in the zonal direction.

The effectiveness of measuring different variables in the tropical ocean was first studied by Philander et al. (1987b) with a general circulation model of the Pacific Ocean. They found that temperature is the most important variable to be defined initially in determining subsequent model evolution. Using model-generated temperature and velocity data, Moore et al. (1987) investigated the effect of updating models of the Indian Ocean. They observed that whether temperature or velocity data are more useful depends on the model's diffusion and viscosity coefficients. For the values used by most ocean models, temperature data are more useful than velocity data. However, increasing the diffusion or decreasing the eddy viscosity results in velocity data being better for determining the model state. These results were ascribed to changes in the energy partitioning from one case to the other, with the ratio of kinetic energy to potential energy being larger in the latter experiments.

By using both analytical arguments and a numerical model, Anderson and Moore (1989) examined the relative information content of mass and velocity measurements for determining low-frequency equatorially trapped waves. They found that mass and velocity data are equally useful for estimating the Kelvin wave, even when dissipation is present, but the Rossby wave adjustment is sensitive to the magnitude and form of dissipation used. Most of the above studies assumed perfect atmospheric fluxes.

It is important, therefore, to investigate the problem of correcting the errors caused by poorly known surface fluxes. Miller and Cane (1989) considered the wind stress error as their model error in constructing a simple covariance function for the Kalman filter scheme and achieved encouraging results. Moore and Anderson (1989) and Sheinbaum and Anderson (1990a,b) have assimilated expendable bathythermograph (XBT) observations into a one-layer linear reduced-gravity model of the tropical Pacific Ocean driven by observed monthly mean wind data. They demonstrated that the XBT data contain large-scale information and improve the model's initial state. They also found that the information from data in the eastern equatorial Pacific cannot be successfully assimilated into the model. Sheinbaum and Anderson (1990b) showed that this problem stems from the inconsistency between the forcing and the data. Some experiments in which model stratification or magnitude of the wind stress were adjusted did not identify clearly the possible cause for this inconsistency.

These authors did not consider the relative usefulness of the different variables in correcting the error due to wind stress. Furthermore, the use of the observed wind stress and observed data in these papers enhanced the realism of the results but did not permit a complete understanding of the assimilation process at work. New observing systems, with different data distribution and error characteristics, are constantly being planned and implemented. Therefore, data assimilation in the presence of wind stress error needs further study, using simulated data and assumed wind stress patterns.

In this paper, we investigate what can be achieved with optimal interpolation (OI)—the data assimilation method most commonly used in NWP (Gandin 1963; Rutherford 1972; Lorenc 1981)—for different wind stress errors. The framework used is that of a perfect model and observations, updating only the model state and not trying to correct the momentum flux itself. Here the error in model-simulated fields caused by the wind stress error is called "simulation error."

Wind stress error can be considered as the combination of two components: systematic error and stochastic error, in both time and space. By examining the performance of OI in these cases, we can determine and understand its ability to correct the simulation errors. We are also interested in the relative importance of thermal and current measurements, and in the importance of their location, for correcting simulation error. These questions are examined here for the tropical ocean only.

The model and assimilation method are described in section 2. In section 3, we explore first the case of switching on a perfect wind stress, and find that the error in the initial state is damped out more or less rapidly for different datasets, given as thermocline depth and zonal velocity observations. In section 4, datasets similar to those used in section 3 are assimilated to correct a systematic wind stress error. The effect of Kelvin and Rossby waves excited during the assimilation process on error reduction is also discussed. The reduction of the simulation error caused by stochastic wind stress errors is presented in section 5; various data types are used here too. Concluding remarks follow in section 6. An appendix gives analytical results.

2. Model and assimilation method

a. Model formulation

A linear shallow-water model modified by the long-wave approximation on an equatorial β plane (Cane and Patton 1984) is employed. The model equations,

linearized about a state of rest with constant mean thermocline depth, are

$$u_t - yv + h_x = F - ru, \tag{2.1a}$$

$$yu + h_y = G, \tag{2.1b}$$

$$h_t + u_x + v_y = Q - rh. \tag{2.1c}$$

The equations have been nondimensionalized in the usual way: the timescale is $T = (c\beta)^{-1/2}$ and the length scale is $L = (c/\beta)^{1/2}$, where $c = (g'H)^{1/2}$ is the scale for wave speeds. Here, g' is the reduced gravitational acceleration due to ocean stratification and is taken equal to 2.0 cm s^{-2}. The mean thermocline depth H is assigned the value of 100 m. A Rayleigh friction with decay time r^{-1} of 200 days has been included. The external forcings F, G, and Q are due to the zonal wind stress, meridional wind stress, and buoyancy flux, respectively. To give some idea of the scaling, if one takes $5 * 10^{-2}$ Nm^{-2} as the basic unit of zonal wind stress, for example, the zonal velocity u would have a basic unit equivalent to 8.8 cm s^{-1}, and the change in the thermocline depth, h, would be 6.3 m.

The model state consists of one diagnostic variable, meridional velocity v, and of two prognostic variables, deviation h of thermocline depth from its mean, and zonal velocity u. Two kinds of observations, u and h, were used during the assimilation runs. We consider zonal wind stress forcing F only, so that $G = Q = 0$.

The model domain is a rectangular basin, with a zonal length of 150 degrees, about the size of the Pacific Ocean, and a meridional extent from 16.5°N to 16.5°S. Boundary conditions are no normal velocity at the northern and southern boundaries, and reflection conditions at the eastern and western boundaries.

With the physical characteristics of the tropical ocean in mind, the low-frequency solution is divided into two parts: an eastward propagating equatorial Kelvin wave and westward propagating Rossby waves. This separation is possible since the vector shallow-water modes $(u, v, h)_k$ form an orthogonal and complete set (Cane and Sarachik 1979).

A zonal grid size of 2.0 degrees and a meridional grid size of 0.54 degrees are used in the numerical scheme. Because high-frequency waves are filtered out by the long-wave approximation, a 10-day time step is employed, which allows efficient integration of the model. The details of the numerical scheme can be found in Cane and Patton (1984). The results of the calculation are given in the model's nondimensional units throughout the paper.

b. *Data assimilation method*

We rely on the so-called optimal interpolation (OI) analysis scheme, which is commonly used at major weather forecasting centers, as well as in a semioperational prediction system for the tropical Pacific (Leetmaa and Ji 1989). The basic idea of OI is to combine the model field and the observed data to estimate the correct field in a way consistent with the estimated accuracy of each (Gandin 1963; Rutherford 1972; McPherson et al. 1979; Lorenc 1981). As the method uses statistical properties of the model and the observations, it is also called statistical interpolation. A brief description follows.

The model value, p_k, at grid point k is taken as the first guess. The analyzed value, a_k, at k is given by adding to p_k a weighted linear sum of the differences between observation and model value, $b_i - p_i$, at the observation points i:

$$a_k = p_k + \sum_{i=1}^{n} w_{ik}(b_i - p_i). \tag{2.2}$$

The weights w_{ik} are determined so as to minimize the estimated analysis error E_k^a,

$$E_k^a \equiv \langle (a_k - T_k)^2 \rangle^{1/2}, \tag{2.3}$$

where angle brackets indicate a statistical mean, and T_k represents the true value at that grid point k.

The true value is defined as the value we wish to estimate in the analysis, which is not necessarily the actual true value. In this paper, it represents the large-scale motion, excluding inertia–gravity waves, mixed Rossby–gravity waves, and short Rossby waves.

The OI scheme requires knowledge of spatial error covariances for the model field and the observations, since the weights needed to minimize analysis error as defined by (2.3) depend on these error covariances. Following Miller and Cane (1989) and Leetmaa and Ji (1989), a Gaussian function with zonal length scale of 10° and meridional length scale of 1.6° is taken as the correlation function for each of the variables h and u.

With two prognostic variables, the best results would be obtained by using a multivariate analysis scheme, which transfers instantaneously information about an observed variable to the other variables. In data assimilation, the geostrophic relation is frequently used to connect mass and velocity updates in the midlatitudes.

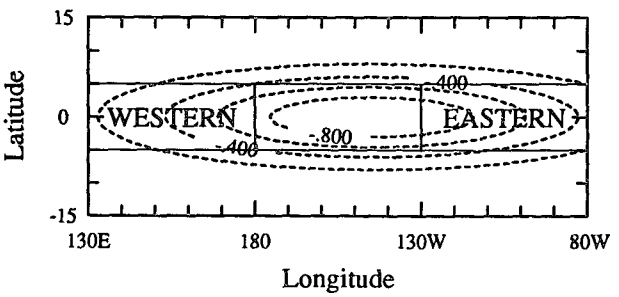

FIG. 1. The wind stress field; the contour interval is 0.2 nondimensional units, with eastward stress positive. The verification regions are surrounded by solid lines and marked by WESTERN and EASTERN for the western and eastern region, respectively.

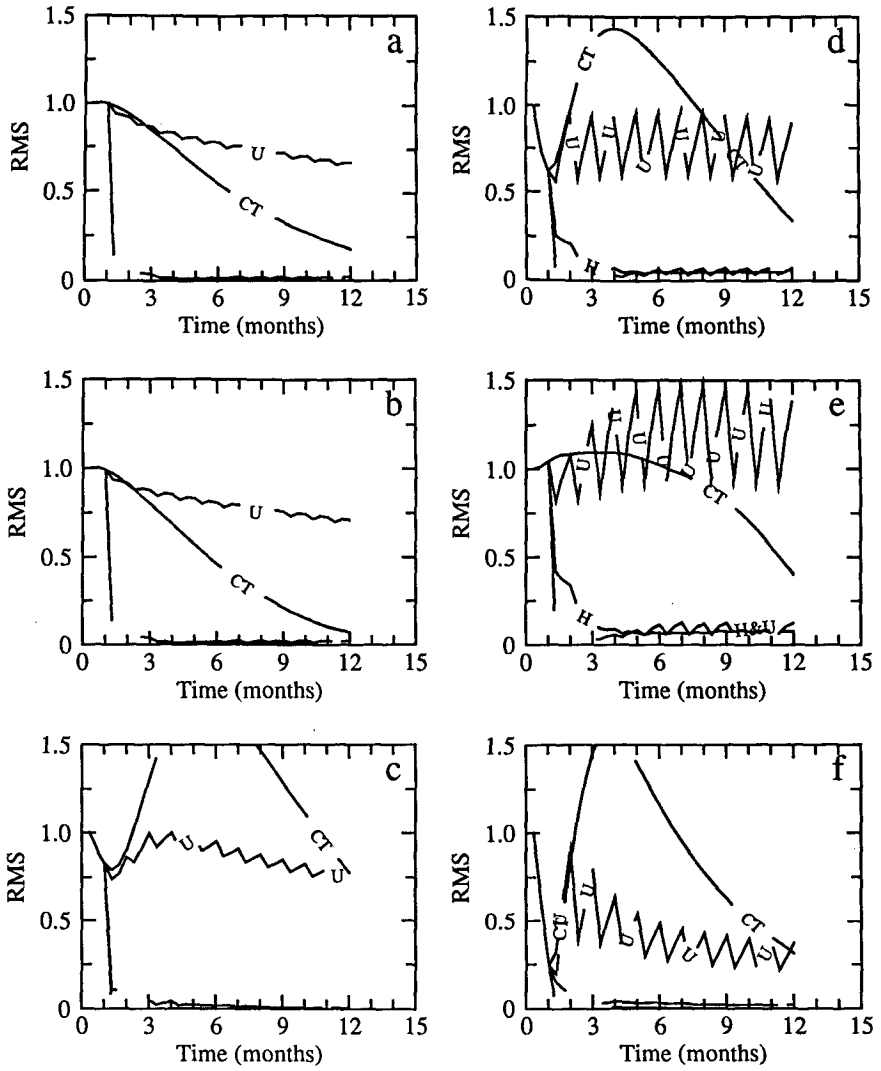

FIG. 2. Normalized rms errors of h (panels a, b, and c) and u (d, e, and f) of the control run (-CT-), and of three assimilation runs with the datasets h&u (-H&U-), h only (-H-), and u only (-U-), where the wind stress has only a timing error: (a) and (d) the entire equatorial band; (b) and (e) the western region; and (c) and (f) the eastern region. Normalization factors are (a) 15.8, (b) 22.9, (c) 4.4, (d) 4.5, (e) 4.3, and (f) 4.4.

However, as the geostrophic relation breaks down near the equator, the cross covariance between thermocline depth and zonal velocity becomes more complicated than that customarily used in midlatitudes. To avoid this complication, a univariate OI scheme has been used for all our experiments, as in Leetmaa and Ji (1989). Information is still transmitted from one variable to another, in the course of the assimilation cycle, by the model dynamics. No initialization procedure was implemented to balance the two analysis fields, since model dynamics lets them adjust to each other in due time, after updating. Further computational savings were achieved by applying the "volume" or "box version" of OI (for details see Lorenc 1981; Hao 1991).

The "observations" used here were model generated and are described in further detail in sections 3–5. Because we were concentrating on the physical processes associated with simulation error correction, no observational error was added to the data. The ratio between observational and model error variance, required for stability of the OI scheme, is assigned the value 0.05 for practical purposes.

Model fields are updated at the end of each month for all the assimilation runs, except where the updating frequency is explicitly stated to be different. An updating interval of one month has been used by many authors in the tropical oceans, given the emphasis on monthly data in the study of El Niño (e.g., Leetmaa and Ji 1989; Moore et al. 1987; Moore and Anderson

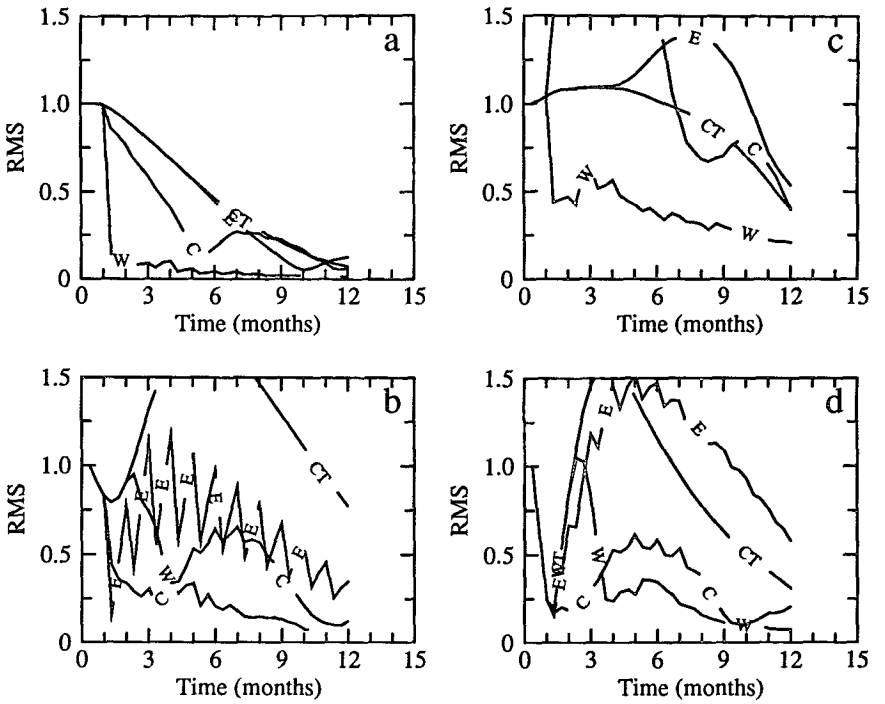

FIG. 3. Normalized rms errors of h (panels a and b) and u (c and d) of the control run (-CT-) and of three assimilation runs with thermocline-depth observations h restricted to: eastern (-E-), central (-C-), and western (-W-) regions. (a) and (c) For the western region; (b) and (d) for the eastern region. Normalization factors are (a) 22.9, (b) 4.4, (c) 4.3, and (d) 4.4.

1989); this corresponds here to three model time steps. The problem of optimizing the updating interval for tropical ocean models is touched upon in the appendix.

Root-mean-square (rms) errors in each variable are used as the main measure of assimilation performance. Total rms error $E(h\&u)$, based on the energy $(u^2/2 + h^2/2)^{1/2}$, is also used in comparing the usefulness of some datasets. To focus on the equatorial ocean, validation is carried out in the band between 5°N and 5°S (cf. Anderson and Moore 1989). To evaluate how the assimilation performs in different parts of the basin, we consider furthermore [following Moore and Anderson (1989)] a western region (120°–170°E), central region (170°E–140°W), and eastern region (140°–90°W) (Fig. 1).

The rms error of the analysis field is zero for many of the experiments, when one or both prognostic variables are observed at every grid point. To make the visualization of results clearer and less dependent on our assumptions of perfect observations, we plot the error curves for the assimilation runs using only the simulation-error value preceding the actual update. The more common convention of showing, at each update time, both this value and the analysis value makes for messy plots, with larger jumps from large simulation-error values to very low (or zero) analysis values. Moreover, it is the analysis error at update time that depends most on the assumptions about observing errors, more so than the simulation errors in between updates.

For convenient plotting, the rms errors are normalized. Different normalization factors are used for the different regions and cases. In section 3, the variances of the reference state for different regions and for the whole equatorial band have been used to normalize the corresponding rms errors of the control and assimilation runs. In section 4, the variance of the simulation error arising from wind stress error is used. In section 5, mean rms errors of the control run for each variable are taken as the normalization factors.

3. Assimilation in the case of perfect wind stress

In this section, we consider the case of the model being forced by a wind stress that is switched on at $t = 0$, remains stationary thereafter, and has zero error. This case can also be viewed as either the wind stress having a timing error or the model state having an initial error. Since any gradual time change of the wind stress can be decomposed into Heaviside functions, the case of a sudden switch on is actually more general than it appears.

The assimilation is useful, as we shall see, insofar as it reduces the time to reach the equilibrium state with respect to the pure spinup case. We tried to determine the relative importance of different observation types and locations.

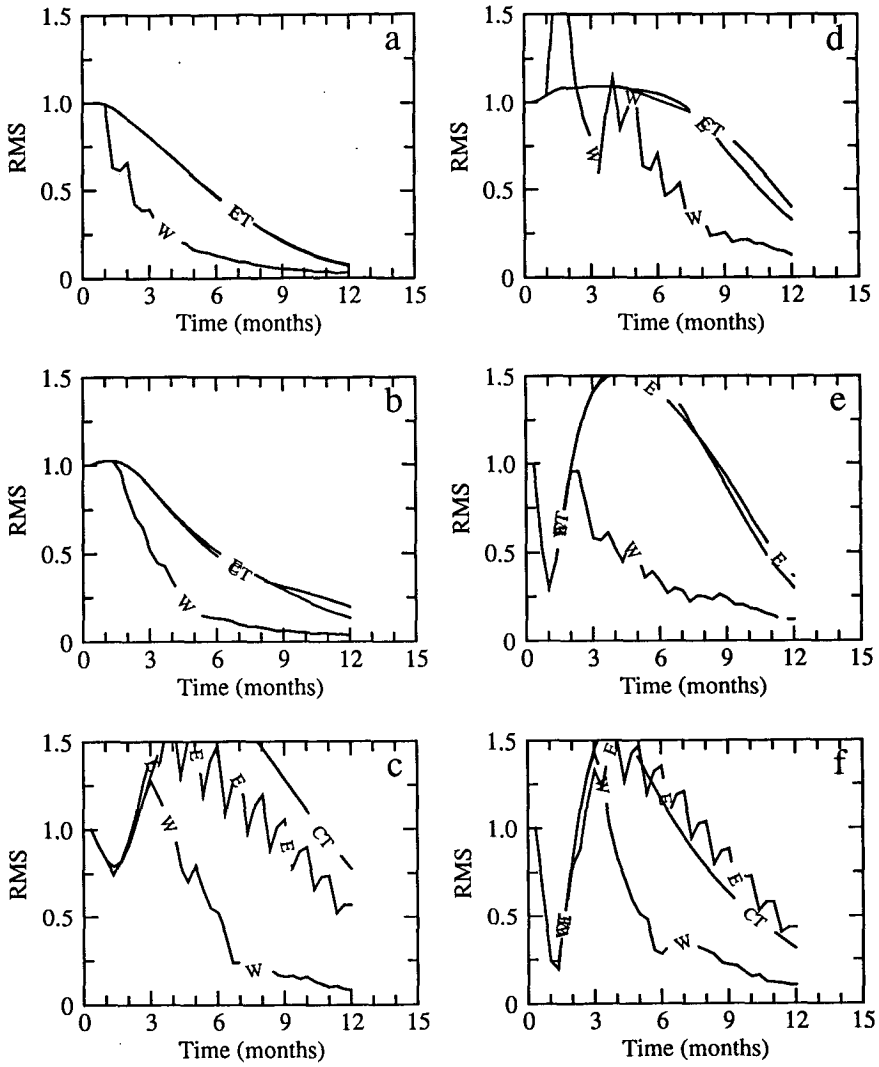

FIG. 4. Normalized rms errors of h (panels a, b, and c) and u (d, e, and f) of the control run (-CT-) and the two assimilation runs with observations $h\&u$ made along a single meridional section: at 140°E (-W-)—i.e., in the western part of the basin—and at 110°W (-E-)—i.e., in its eastern part—respectively. (a) and (d) For the western region; (b) and (e) the central; and (c) and (f) the eastern regions. The normalization factors are (a) 22.9, (b) 14.7, (c) 4.4, (d) 4.3, (e) 4.7, and (f) 4.4.

A westward zonal wind stress is used here with its maximum at 145°W on the equator, and decaying exponentially away from this maximum, with different length scales in the zonal and the meridional direction (Fig. 1). The control run was a spinup experiment starting from a state of rest and zero thermocline depth anomaly. The true state is thus the equilibrium state corresponding to the constant wind stress. The observations were taken from the true state.

The stages involved in the spinup of the tropical ocean basins are well understood, having been documented by Cane and Sarachik (1979) and Philander and Pacanowski (1980), among others. The spinup process involves an initial acceleration of surface waters by the wind, followed by excitation of a Kelvin wave at the western and of Rossby waves at the eastern boundary, with subsequent eastward and westward propagation, respectively. In addition to the fast Kelvin wave and slow Rossby waves excited initially, the Rossby waves and Kelvin waves resulting from the reflection of the initial waves affect the adjustment of the equatorial ocean.

The adjustment due to the Kelvin and Rossby waves allows the ocean to slow the initial acceleration and sets up a zonal pressure gradient across the basin; that is, a slope in the initially horizontal thermocline. This slope is given by the forced balance between the pressure gradient and zonal wind stress along the equator,

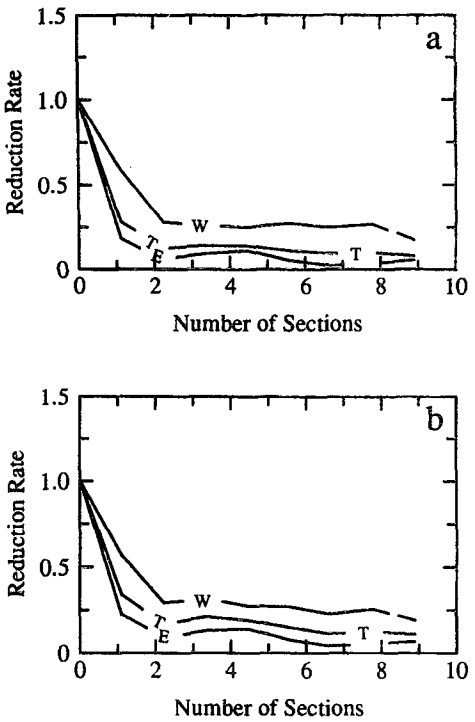

FIG. 5. Reduction rates of h error (a) and of the total error (b) after 1-yr assimilation runs with $h\&u$ data at an increasing number of meridional sections. The curves are the relative errors for the entire equatorial band (-T-), the western (-W-), and the eastern region (-E-).

$h_x = F$, which is also called "Sverdrup balance." The spinup time scale of the model is about 18 months [see Fig. 3.2 in Hao (1991) and discussion there]. An interesting point is the overadjustment of both h and u fields during months 2–9 after the switch on, a problem that appears in the increase of rms errors after the initial decrease (see Fig. 2).

a. Relative importance of observed fields

To determine the relative importance of h and u observations, three datasets were assimilated into the model. They are observations of h only, u only, or both h and u ($h\&u$) at all grid points of the entire basin.

Figure 2 shows normalized rms errors of h and u, $E(h)$ and $E(u)$, during the first 12 months of the control and assimilation runs. The OI scheme combines the information from both the model forecast and the observations, and the relative contribution of the two within the analyzed fields depends approximately on the ratio of the observational to the model-error variance. With perfect observations for all the variables and at all grid points, the OI method brought the model state to equilibrium in just one assimilation cycle. This result proves that the small value assigned the ratio of the observational to model error variance is appropriate, and the OI scheme works. The small adjustment after the first assimilation step comes from the smoothing effect of OI, which gives a somewhat different spatial scale than the true state.

Observations of h are much more useful than those of u in this case, since the most important consequence of the equatorial ocean's adjustment to wind stress is the balance between pressure gradient and zonal wind (Cane and Sarachik 1979; Philander 1990; Sheinbaum and Anderson 1990b). Therefore, the assimilation run with h observations reaches the equilibrium state soon after its pressure gradient is given the correct value by the first update. After updating h several times, the rms errors in the u field become negligible. This result indicates that a large amount of h information has been transferred to the u field by the model dynamics. The overadjustment problem has been completely eliminated with h observations.

In the run with u data only, the assimilation is successful only in the eastern region, compared to the control run (Figs. 2c,f), and diverges elsewhere. Because the guess fields instead of the analysis fields are used to calculate the rms errors, the assimilation error is not zero at the updating time step and becomes quite large at the next step due to the adjustment forced by the wind stress and between the variables. The sawtooth shape of $E(u)$ in Figs. 2d–f indicates some rejection of u information during the model adjustment, and strong month-to-month variability due to the monthly updating. During the early stages of the assimilation (for about 3–4 months), the u observations did improve the h field (Figs. 2a–c). In the western region, u observations perform poorly because updating u disturbs the processes that establish the correct thermocline slope and excites spurious Kelvin waves at the western boundary. Thus, u observations are only valuable in the eastern region to correct overadjustment (Figs. 2c,f).

The greater usefulness of h observations can also be explained in terms of the system's energy partitioning between potential energy (PE) and kinetic energy (KE). This division was highlighted for a tropical ocean case by Moore et al. (1987) and by Anderson and Moore (1989). Since the meridional velocity of this model is not a prognostic variable and its value is gen-

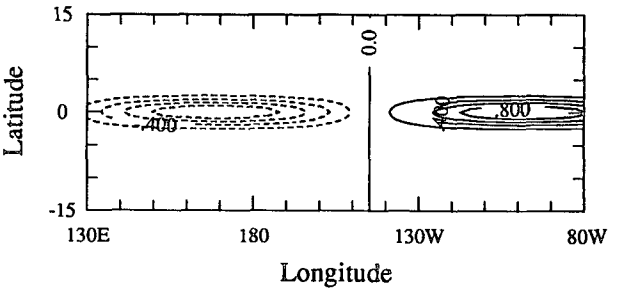

FIG. 6. Wind stress as in Fig. 1 but for the systematic error case.

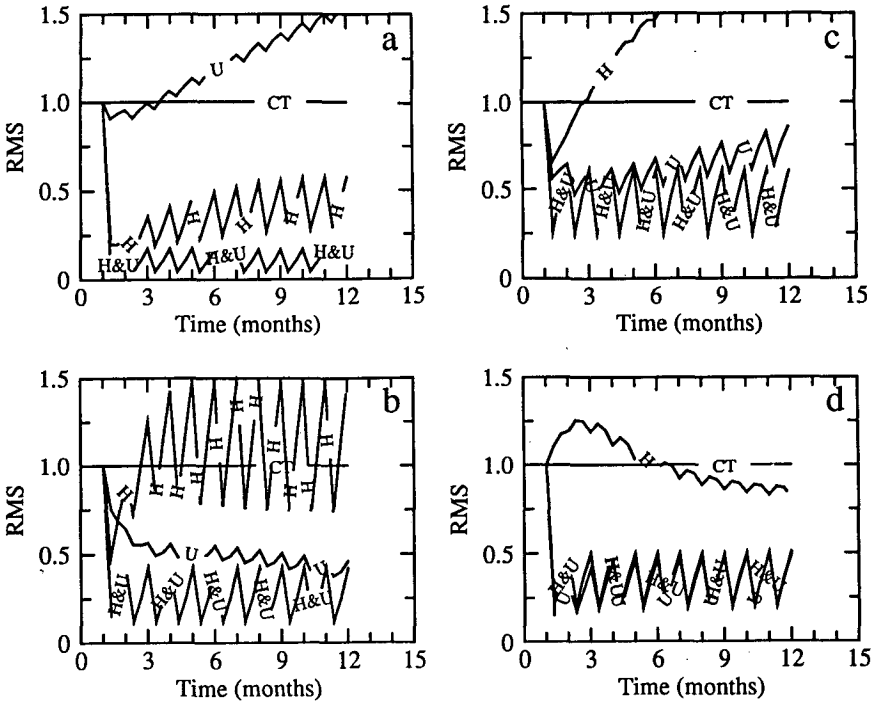

FIG. 7. Normalized rms errors of h (panels a and b) and of u (c and d) for the systematic error case. The curves are labeled as in Fig. 2. (a) and (c) The western region; (b) and (d) the eastern region. Normalization factors are (a) 12.1, (b) 3.6, (c) 6.7, and (d) 8.5.

erally small, we did not account for it in calculating the KE here. In a nondimensional shallow-water model, the PE and KE per unit mass of the equilibrium state (h, u) are just half the total mean variances of the reference h and u, which are 125.0 and 10.4, respectively. Thus, averaged over the whole equatorial basin, potential energy comprises about 92% of the total energy in this case. When the model is updated by h observations at all grid points, the dynamical processes need to convert only a little PE to spin up the balancing field of KE. Hence, there are just small differences in rms errors between the assimilation runs with datasets of $h\&u$ and of h only in Fig. 2.

b. *Role of location of observations*

To determine how the location of measurements affects the assimilation, a set of experiments was conducted with h observations at different zonal locations: restricted to the western, central, or eastern region as defined in section 2. Figure 3 shows that data in the western region produce the greatest improvement in all regions for both fields (the results for the central region are similar to the western one, and not shown). Right after the first h updating in the western basin, the h errors there become negligible. After the first updating in this run, the error curves of both h and u in the eastern region differ from the control run at one month. Since the Kelvin wave takes about one month to move from the western into the eastern region, the updating information in the west seems to be carried to the east in the form of Kelvin waves. Small improvement of h and worsening of u with h data from the eastern region indicates that little information from the observations has been propagated westward (Figs. 3a,c); this paucity of information traveling westward might come from the relative slowness of the Rossby waves carrying it, compared to the rate of error growth due to the forcing.

The effect of depth observations in the central region is mixed for u error in the other two regions. The updating has largely improved the spinup of the u field in the eastern region (Fig. 3d), but disturbed the field in the western region (Fig. 3c). The imbalance between the observed and unobserved areas excites the signal to be assimilated. When the observations are in the central basin, one would expect that this signal consists of the relatively fast eastward propagating Kelvin wave generated near its eastern side and a relatively slow westward propagating packet of Rossby waves at the western side. Thus, the adjustment of the u field in the western region is hampered by the slowness of the assimilation signal propagating into it.

To understand better the zonal propagation of the updating information, we have carried out two assimilation experiments with observations of h and u at all the grid points along a single meridional section. It extends from the northern to the southern boundary

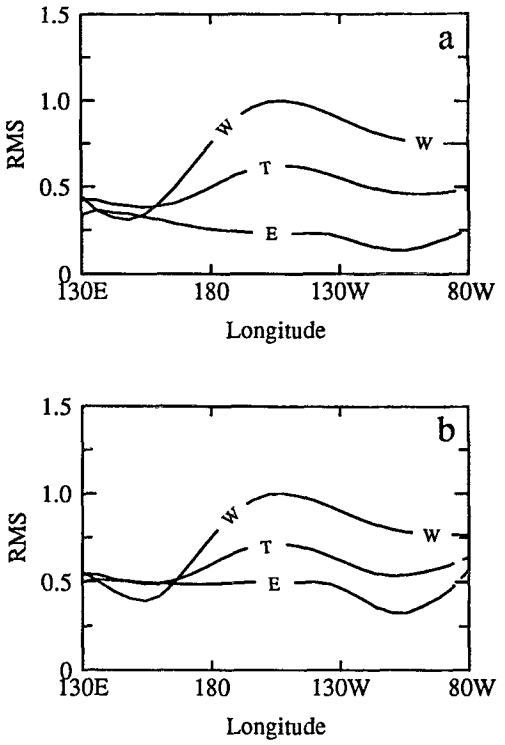

FIG. 8. Normalized rms errors of h (a) and of total field (b) after 1-year assimilation runs with $h\&u$ data along a single meridional section. The rms error is plotted as a function of the zonal location of the section. The curves are labeled as in Fig. 5. Normalization factors are (a) 16.0 and (b) 12.7.

of our basin at 140°E and 110°W, respectively. Due to the OI weights, the immediate impact of these observations on the analysis field is not limited to the line of observations, spreading instead through the basin by about 10° longitude in both zonal directions.

By comparing the rms error curves of these two assimilation runs with those of the control run, we can follow the propagation of the updating information (Fig. 4). We find that Kelvin waves are excited preferentially by updating the depth and velocity along the western section (at 140°E). This excitation yields a faster spinup process on their way east. Differences between the control and assimilation run when observing along the eastern section (110°W) are small in the western and central regions (Figs. 4a–d); this small difference indicates that the Rossby waves excited preferentially by the updating of the eastern section of observations had only a small effect on their way west. The contrast in the impact of the two single sections suggests that eastward propagation of the updating information is preferred by the model, a preference anticipated from the difference between the wave speeds. Subject to the same damping rate, the faster wave retains a stronger signal than the slower ones, after traveling the same distance.

Experiments have also been carried out to study how many $h\&u$ observations are adequate for this case. Figure 5 shows the rms errors of h and total rms errors of the assimilation runs with data taken at an increasing number of equally spaced meridional sections, from 1 to 9. It shows that even one data section can help the ocean spinup processes improve dramatically. On the other hand, the gradual reduction in the rms errors when increasing the number of sections shows the benefit of more data. The evidence that error curves are very flat after two sections suggests that this number might suffice to correct errors in the initial state only, at least for the very simple dynamics of this low-resolution model. Figure 5 also shows that the error reduction rate is larger for the eastern than the western region.

4. Correction of systematic wind stress errors

The case we study here is that of constant wind stress error, which could be caused by constantly under- or overestimating the atmospheric wind speed. The model's linearity allows us to 1) define a state of no motion and zero thermocline anomaly as our true state, and 2) force the model with the error in the wind stress only. The more the model fields depart from the state of rest and horizontal thermocline, the larger the model error is.

Before we discuss the assimilation runs, the propagation of an initial thermocline depth disturbance may help us understand the wave activities excited by updating observations in the later experiments. Philander et al. (1984) showed that an initially bell-shaped thermocline displacement breaks into an eastward-traveling Kelvin wave and a westward-traveling Rossby wave packet. We can think of the difference between the analysis field and the wind-induced equilibrium state as a sum of such displacements of thermocline or current; each update will excite these two types of waves. The gradual assimilation of data in this section represents just the superposition of similar waves generated by each small subset of the data at different locations during each update.

The zonal wind stress error (Fig. 6) has a sinusoidal dependence on longitude, and is exponentially decaying to the north and south away from the equator. The initial state for all the runs in this section is the equilibrium state induced by the prescribed wind stress error and gives a constant error for all times if no data are assimilated. To examine the relative usefulness of observations for correcting systematic wind stress error, we assimilated three datasets—h, u, and $h\&u$—observed at all grid points (Fig. 7).

Assimilation of the dataset $h\&u$ reduced the averaged $E(h)$ to about 10%–25% (in the western to eastern region, respectively) and $E(u)$ to 30%–40% of the control run in all parts of the basin (not all shown). Updating h only has reduced $E(h)$ but increased $E(u)$ for the

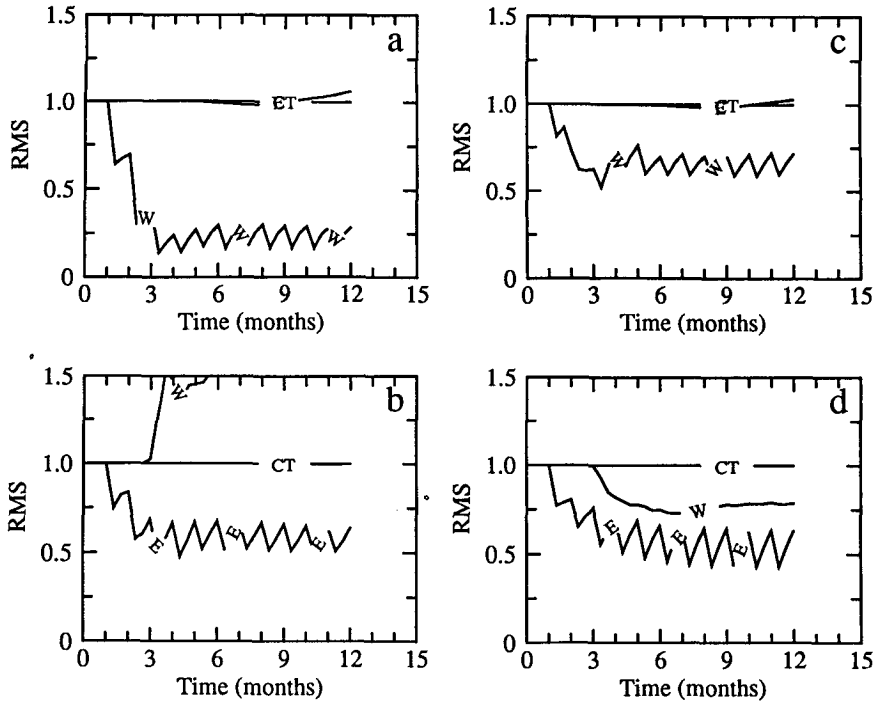

FIG. 9. Normalized rms errors of h (panels a and b) and u (c and d) as in Fig. 4 but for the systematic wind stress error case. Panels and normalization factors as in Fig. 7.

entire equatorial area (not shown, similar to the western region).

The impact of h data differs for each area. The h data reduce $E(h)$ to less than one-half of the control run's in the western region (Fig. 7a). However, depth information is lost very quickly in the eastern basin, as the model thermocline is restored to oscillate around the wind-induced equilibrium state (Fig. 7b). The difficulty of improving model depth field over the eastern equatorial ocean with depth data was also noticed by Sheinbaum and Anderson (1990a,b). They attributed this deficiency to the mismatch between their model, wind stress, and observations. Large $E(u)$ occurs because the velocity field error is driven directly by the erroneous wind stress, and the information transfer from h data is less efficient. By updating h only, hardly any net correction to the u field in the eastern basin (Fig. 7d) occurs, while the error $E(u)$ diverges in the western region (Fig. 7c).

Velocity data are useful in the eastern and central region. In terms of the total rms error $E(h\&u)$, u data lead to larger errors than h data (not shown). In short, depth data have a strong positive impact only on the thermocline depth in the western region, while the zonal current data improve both h and u fields in the other two equatorial regions [see Hao (1991) for central region].

For this systematic error case, the effect of observational location was also studied. The observations used are $h\&u$ along a single meridional section at various zonal locations. The averaged $E(h)$ and $E(h\&u)$ after 12-month assimilation runs are presented in Fig. 8. It shows that, when validating over the entire equatorial band, both rms error in h and total rms error are smaller when the section is at either side and larger when it is in the middle of the basin; placing observations in the western basin will produce the greatest improvement. Observations are still most useful for the local area in which they are taken: the errors for the western region have a lowest point when the section is there, and likewise for the eastern region.

To understand better the zonal propagation of the updating information in this case as well, we study in more detail two particular assimilation runs among the previous experiments: one section is in the western, the other in the eastern region. The rms errors for the two assimilation runs and the control run are shown in Fig. 9. Updating the western section data increased $E(h)$ and decreased $E(u)$ in the central (not shown) and eastern regions (Figs. 9b,d). The increase of $E(h)$ in the eastern region (Fig. 9b) suggests that information about one region does not guarantee benefit in another. The eastern section data improved the simulation error in the central (not shown) but not in the western region (Figs. 9a,c).

The impact of data along a western section on the eastern region, when beneficial, exceeds that of eastern data on the western region. This can be due to one of two reasons: either the model is more efficient in propagating the information eastward or

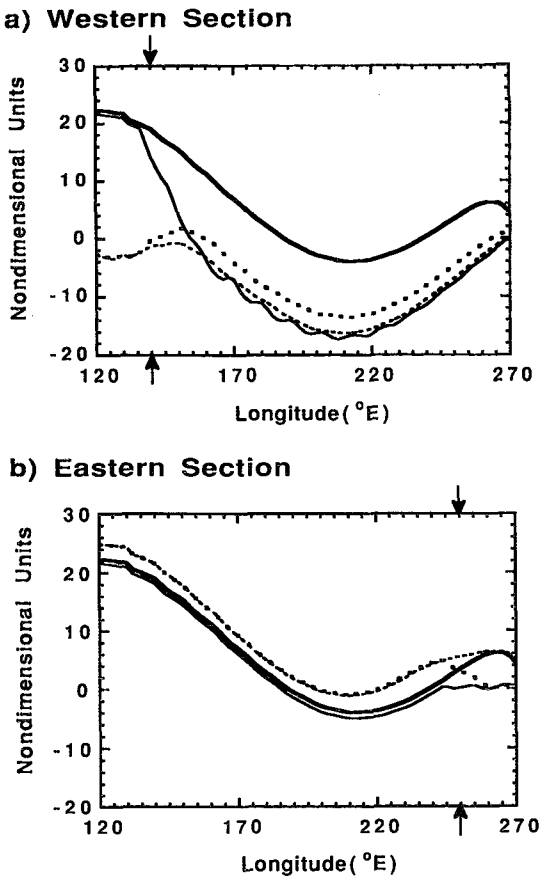

FIG. 10. Thermocline depth anomaly along the equator, with only one meridional section of data *h&u*: (a) the western and (b) the eastern section. Location of either section is shown by arrows in the corresponding panel. The dark solid line corresponds to the control run and dark dashes to the assimilation run with *h&u* data. Light dots and light solid lines show the results of assimilation runs with *h&u* data projected on Rossby waves and the Kelvin wave, respectively. Units are nondimensional and the positive contours represent a deeper thermocline than the mean.

the position of the wind stress error maxima with respect to the data section matters.

More generally, the mixed results obtained with a single section and constant wind stress error suggest that data from a single meridional section cannot correct the entire slope of the thermocline: only the thermocline depth near the updating line is corrected. The depth in other parts of the basin is simply leveled or pushed down with the same thermocline slope maintained by the wind stress. A similar argument was proposed by Sheinbaum and Anderson (1990b) to elucidate their result that using data in the eastern or western equatorial region only was not so successful. Figures 10a,b show the equilibrium thermocline depth along the equator when updating every time step, to avoid the adjustment between the updates. The thermocline profiles shown demonstrate that the observations can only change the slope within the range of influence of the section, given by OI. Clearly, updating along the western section (Fig. 10a) improved thermocline depth in the western part of the basin, but deteriorated it in the eastern part, as the thermocline is simply displaced downward.

Effects of the tropical waves on slope correction are also examined by projecting the *h&u* updating information onto the Kelvin or Rossby waves structures, respectively [see sections 2a and 4 of Hao (1991) for details]. The Kelvin wave information elevated the thermocline to the east of the updating region. The Rossby waves elevated not only the portion of the thermocline west of the updating region, but also the eastern part. These results suggest that the oceanic waves adjust the thermocline in the areas not directly updated by the data, to match the updated region. Given data from a single section, there is little information carried by the waves to faraway regions about the right state. Therefore, correction by the excited waves simply reduces the difference between the area concerned and the data-rich area.

Experiments have been carried out to study the effectiveness of increase in data coverage. Figure 11 shows $E(h)$ and $E(h\&u)$ after one year of assimilation runs with *h&u* data taken along an increasing number of meridional sections that equally divide the ocean basin. With only one section of data at the basin's center, the assimilation run has even larger errors than the control

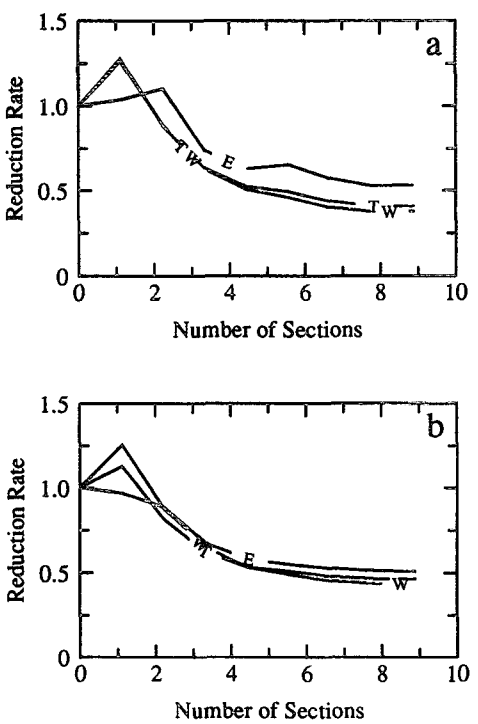

FIG. 11. Reduction rates of h error (a) and the total error (b) as in Fig. 5 but for the systematic wind stress error.

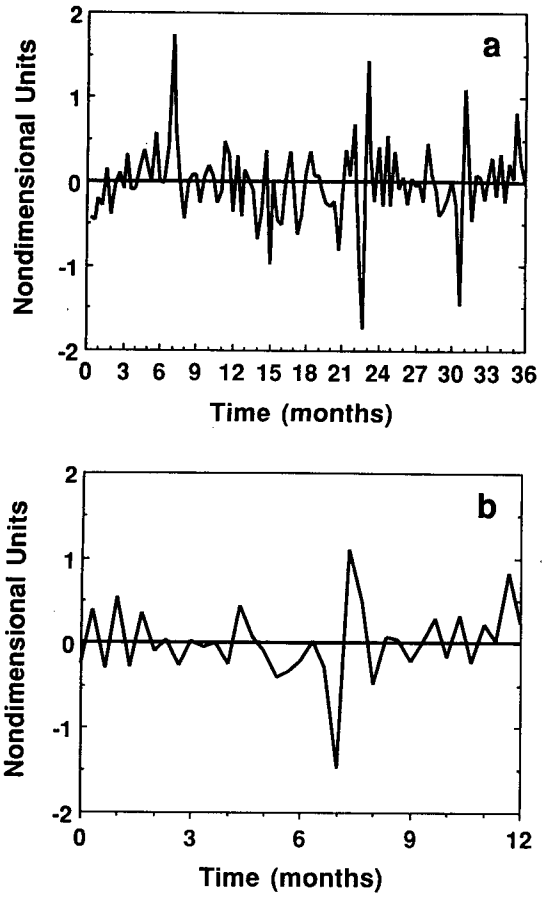

FIG. 12. Three-year realization of the stochastic zonal wind stress at the grid point of maximum variance. (a) The full three years; (b) the last year of the three, which is used during the assimilation run shown in Fig. 13. Stress units are nondimensional.

run, due to the thermocline-slope effect discussed above. By increasing the number of sections, the errors drop sharply. With four sections of *h&u* data, errors for the whole equatorial band are reduced to half of those with no data. Once the number of data sections exceeds four, all the error curves become flat, suggesting that a much denser observation network might be needed to reduce the errors to a desired level. Errors for the western region drop faster than for the eastern region, especially in the depth field (Fig. 11a).

5. Correction of stochastic wind stress errors

Our stochastic model for zonal wind stress errors is similar to that of Zebiak (1989):

$$F(x, y, t) = A[R(t) + R(t - \Delta t)] \times \cos[\omega_0(t + t_0)] \times \exp\left[-\left(\frac{y}{2.5°}\right)^2\right] \exp\left[-\left(\frac{x - x_0}{25.0°}\right)^2\right], \quad (5.1)$$

where R is a normal random variable with zero mean and unit variance, and t_0 represents a uniform random variable on $(0, 2\pi)$. The parameters ω_0 and x_0 were taken to be $2\pi/40$ day^{-1} and 148°E, respectively, and the amplitude A as 0.5 nondimensional units. The forcing function used here has a smaller spatial scale and shorter temporal correlation than that used by Zebiak (1989). Figure 12 shows a three-year realization of $F(x, y, t)$ at $x = x_0$ and $y = 0$, as a function of time; the last year is also shown in greater detail.

The model was forced to spin up by this random wind stress for two years. After the spinup, the fields are updated at the end of each month in an assimilation run. Again, the observations are taken equal to the mean equilibrium state, namely, zero, and the simulation field is that induced by the erroneous wind stress.

Figure 13 presents $E(h)$ and $E(u)$ for the control run and the assimilation run with *h&u* data at all grid points. In the eastern region, far from the forcing area, $E(h)$ and $E(u)$ were corrected down to a marginal level by the updating (Figs. 13b,d). As the signal of the wind stress errors is carried eastward by fast Kelvin wave packets, the small error there suggests that frequent updating effectively counteracts the erroneous wind stress forcing.

For the assimilation run, the peaks of the rms error relate to the occurrences of amplitude maxima of the wind stress error (e.g., months 6.5–7.5 in Fig. 13b); near these maxima, the assimilation performs poorly in the region underneath the wind stress error. Large $E(h)$ and $E(u)$ at the end of month 7 indicate that much updating information has been lost due to the wind burst. When the wind stress is weak, data assimilation works very well, for example, the months 2–3 and 8.5–11 in Figs. 12 and 13. During these time intervals, assimilating observations has greatly helped to reduce the rms error of both variables, as in the case of switch-on perfect wind stress (section 3).

Table 1 gives averaged rms errors over a two-year period for the control run, assimilation runs with *h&u* data, *h* data, and *u* data. The data were observed at all grid points, and the assimilation runs were extended for two years beyond what is shown in Figs. 12 and 13.

For the whole equatorial region, assimilating *h* data reduced $E(h)$ to about half of the control run value, and two-thirds for $E(u)$. By assimilating *u* data, the improvement was larger for the *u* field and lesser for the *h* field than that with *h* data only. The assimilation runs with observations of *h* or *u* only yield total errors, $E(h\&u)$, of about the same magnitude.

To check the effect of the equatorial waves during assimilation, two other assimilation runs were performed with processed datasets: Kelvin wave–projected *h&u* (HU–KP) and Rossby wave–projected *h&u* (HU–RP). The averaged rms errors for these two runs are also listed in Table 1.

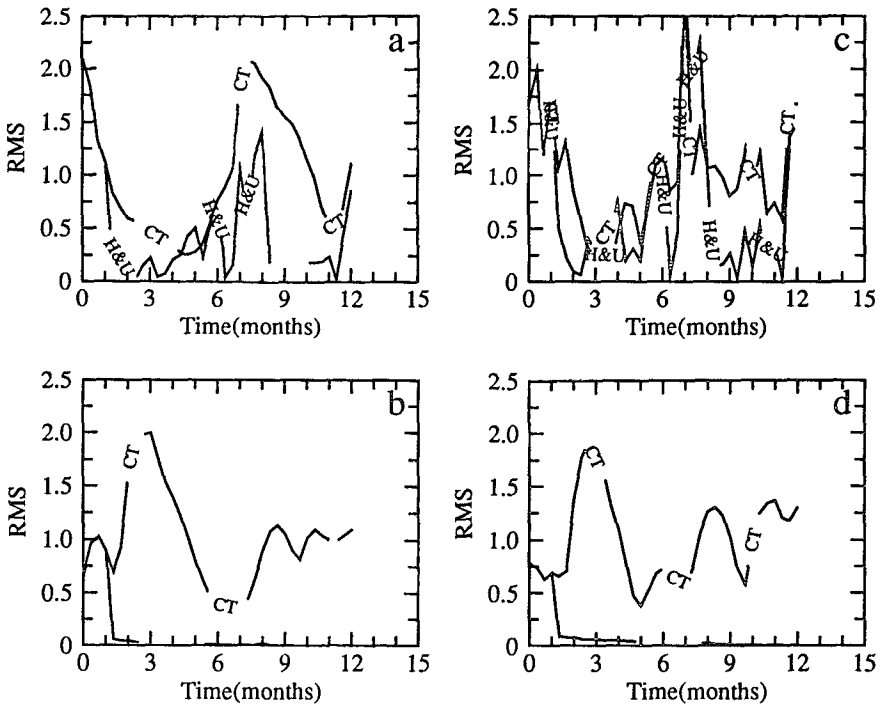

FIG. 13. Normalized rms errors of h (panels a and b) and u (c and d) as in Fig. 7 but for a stochastic wind stress error centered over the western region. Normalization factors are (a) 0.96, (b) 0.66, (c) 0.96, and (d) 0.61.

The improvement made by the assimilation of HU–KP data was much larger than that of HU–RP in the central (not listed) and eastern region outside of the directly forced region. This indicates the efficiency of the eastward propagating Kelvin mode in correcting simulation error caused by the random wind stress error to the west. Such a result could be anticipated from the wave propagation properties. In the western part of the basin, the Rossby wave–projected information had larger impact than the Kelvin wave–projected one. That the HU–RP experiment has smaller errors of both h and u than the control run in the eastern region suggests that some updating information has been reflected eastward by the western boundary.

Results from a set of experiments with a random wind stress error centered in the eastern part of the basin are given in Table 2. It shows that now observed Rossby wave information plays as important a role as Kelvin waves in the previous case. However, the improvement made with HU–KP data is limited for this case.

The impact of the data coverage is also tested for this case of stochastic wind stress error. The datasets are $h\&u$ data at an increasing number of meridional sections, as in sections 3 and 4. Figure 14 presents the averaged total rms errors for the wind stress error being centered in either the western (panel a) or the eastern (panel b) basin. It shows that, when increasing the number of data sections, error is reduced rather slowly for a directly forced region, like the western region in the top panel, and faster for an indirectly forced region. Slow error decrease for the whole equatorial region is due to the larger contribution from the directly forced region. The total error for the whole equatorial band, after two years of assimilation, for the run with nine data sections is about 75% of that without data assimilation for both cases. It appears that the wind stress error occurring in the western region needs slightly fewer observations than that in the eastern region. For the case of a systematic wind stress error, the corresponding error reduction rate (Fig. 11) seems to fall in between the curves for the directly and indirectly forced region.

6. Summary and discussion

A linear shallow-water model with long-wave approximation has been used to study how data assimilation reduces the simulation errors due to three types of wind stress errors. A relatively simple optimal interpolation (OI) method was used to assimilate the data.

The case of timing error for a perfect wind stress is equivalent to that of an error in the initial state. In this case, we found that data assimilation very efficiently brings the model state into equilibrium with the wind stress, when using observations that include measurements of thermocline depth h. Kelvin wave activity,

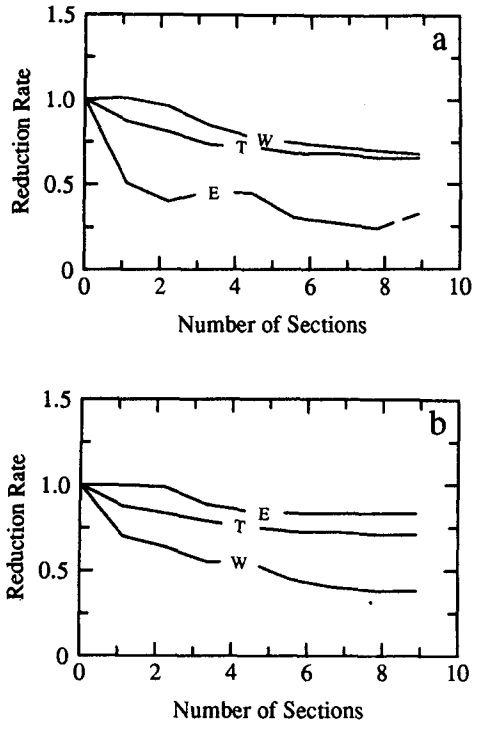

FIG. 14. Reduction rates for total rms errors of two-year assimilation runs with *h&u* data at an increasing number of meridional sections, with stochastic wind stress error centered in the western (a) or eastern (b) region. The curves are labeled as in Fig. 5.

due to its fast wave speed, seemed essential to the success of data assimilation in this case. Observed thermocline depth in the western part of the basin is the most useful in speeding up the model ocean's adjustment from initial imbalance along the equator. We have also observed that velocity data u are useful only in the eastern part of the basin [as suggested by Philander et al. (1987b)]. It seems that two meridional sections of depth and velocity data are sufficient when the wind stress has a timing error only.

When the wind stress has a systematic error, the assimilation counters its contribution to the simulation error. Consequently, the model state asymptotes in time to an oscillation, which results from the balance between the erroneous wind stress and the updating with correct data. Using observations of both variables, h and u, every month at all grid points, data assimilation reduces substantially the simulation error. With observations of one variable, h or u, error reduction for the observed field is reasonably good, but very poor for the other. In a short time, less than a month, wind stress forces u first, then the h field adjusts to it; thus updating h is less efficient in this case. The suggestion that, in general, velocity data carry more information near the equator than depth data do was made first by Anderson and Moore (1989); they argued that, to zeroth order, kinetic energy is concentrated near the

TABLE 1. Two-year averaged rms errors of the control run (CNTRL), as well as for assimilation runs with datasets of h & u (HU), h only (H), u only (U), Rossby wave-projected h & u (HU-RP), and Kelvin wave-projected h & u (HU-KP). Stochastic wind stress error is centered in the western region.

		CNTRL	HU	H	U	HU-RP	HU-KP
Rms error of h	Western	1.105	0.381	0.564	0.728	0.520	0.863
	Eastern	0.593	0.040	0.148	0.194	0.456	0.063
	Entire	0.887	0.244	0.397	0.511	0.566	0.522
Rms error of u	Wester	0.927	0.621	0.876	0.730	0.713	0.796
	Eastern	0.557	0.042	0.204	0.112	0.429	0.071
	Entire	0.812	0.392	0.624	0.485	0.655	0.492
Total rms error	Western	1.041	0.526	0.748	0.752	0.635	0.851
	Eastern	0.580	0.043	0.181	0.161	0.444	0.069
	Entire	0.857	0.33	0.529	0.511	0.616	0.521

equator, while potential energy is concentrated off the equator for the planetary waves. However, the relative usefulness of h and u also depends on the updating interval, the wind stress error scale, and the dissipation or damping in the system (see appendix; Moore et al. 1987; Moore and Anderson 1989).

Correction of the thermocline slope is limited to the vicinity of the updating area, for realistic wind stress amplitudes. Outside of this region, the slope is balanced by the wind stress. This result suggests the importance of wider data coverage to correct a systematic wind stress error. The experiments for coverage by *h&u* data show a very small reduction by increasing the number of meridional data sections over four. To reach a reasonable error level will require fairly dense observations.

For both the switch-on case and the case of systematic wind stress error, experiments with *h&u* data sections have shown that information about a single location or small area may degrade the estimated state at other locations. The question of how to use observations in one area to produce consistent improvements in other areas is still open, at least for OI.

The impact of Kelvin and Rossby waves excited by the updating process in the presence of a systematic

TABLE 2. As in Table 1 but with a stochastic wind stress error centered in the eastern region.

		CNTRL	HU-RP	HU-KP
Rms error of h	Western	0.455	0.076	0.390
	Eastern	0.535	0.327	0.509
	Entire	0.555	0.223	0.509
Rms error of u	Western	0.332	0.065	0.286
	Eastern	0.800	0.595	0.787
	Entire	0.657	0.378	0.635
Total rms error	Western	0.414	0.072	0.345
	Eastern	0.693	0.493	0.676
	Entire	0.618	0.319	0.581

wind stress error is complex. In particular, the propagation of these waves does not change thermocline slope outside the updating area. Unlike the inertia–gravity waves in atmospheric models, whose effect on OI is always deleterious (Daley 1981; Ghil 1989), Kelvin and Rossby waves can have either positive or negative effects on reducing simulation error, depending strongly on the wind stress error pattern. That pattern affects the sign of the simulation errors at various locations (see also Moore 1990).

In the case of stochastic wind stress error, updating both h and u fields reduces the simulation errors greatly in the unforced region. In the forced region, it reduces them to about one-third for the thermocline depth, and two-thirds for the current. The relative importance of the Kelvin and Rossby waves excited by the updating depends on the location of the forced region. If forcing is concentrated in the western part of the basin, Kelvin waves play a crucial role in correcting simulation error. On the other hand, Rossby waves are important when the forced region is located to the east. Our results indicate that correcting stochastic wind stress errors requires more data than correcting systematic errors.

In a number of experiments with partial data coverage, whatever the nature of the wind stress error, Kelvin waves were more efficient in carrying the observational information eastward than were the Rossby waves in carrying it westward. This appears to be due to the fact that, at equal damping rate, the higher speed of the Kelvin wave carries more information farther away from the observed area. As a consequence, better observational coverage in the western part of a given tropical ocean basin appears preferable.

When the simulation error arises from the initial state only, two meridional sections appear to suffice in correcting for the error. The equatorial waves propagate zonally, back and forth, through the sections, permitting successive observations of thermocline depth and slope, as well as current. Asymptotic error reduction by OI is thus slower than for the truly optimal sequential filter (Ghil et al. 1981; Ghil 1989), but considerably faster than for pure spinup.

The case of systematic and of stochastic wind stress error are successively harder, as the information on the true state provided by the data has to counteract sustained, persistent misinformation fed by the forcing into the simulation error. It is natural, therefore, that a larger number of meridional sections is necessary to achieve satisfactory results. In practice, simulation error contains all three components studied here separately in sections 3–5. It follows that the number of sections provided by the full TOGA TAO array (Hayes et al. 1991) should be barely sufficient to provide subsurface information to a multilevel general circulation model for the tropical ocean. The array might give, however, fully satisfactory results (cf. Miller 1990) for a simpler, reduced-gravity ocean model, with one or two active layers, when more advanced data assimilation methods are used.

The results presented here have to be viewed with considerable caution, due to all the simplifying assumptions about the model and observations. Still, our results do show that OI can reduce, in a tropical ocean model, simulation errors due to both initial and wind stress errors. While these results might appear too optimistic, owing to the simplifying assumptions, there are two considerations that could compensate for this. First, the larger role played by the subsurface state in a multilayer model enhances the importance of internal data relative to the external forcing. Second, nonlinear models are likely to be less sensitive to wind stress than linear ones (Périgaud and Delecluse 1989).

Given the most favorable conditions, that is, perfect model and perfect observations with complete coverage, the limited success of OI in counteracting stochastic wind stress error persuades us to search for more powerful methods. Changing the wind stress so as to agree better with the estimated state of the ocean is one promising avenue of giving internal data greater weight in regions of forcing. Parameter estimation and stochastic control theory, combining features of stochastic estimation and deterministic control (Gelb 1974; Wunsch 1988; Tziperman and Thacker 1989; Daley 1991; Ghil and Malanotte-Rizzoli 1991), should provide the basic ideas for modifying the wind stress. The computational problems posed by such an approach may be overcome with local approximations in space and time, by dividing a large system into many small subsystems.

Acknowledgments. We wish to thank J. D. Neelin for many useful discussions and F.-f. Jin, D. Halpern, and C. R. Mechoso for valuable comments. The presentation was greatly improved by the constructive comments of two anonymous referees. This work was supported by ONR Grant N00014-89-J-1845, NASA Grant NAG-5317, and NOAA Grant NA26GP0114-01.

APPENDIX

Analytic Results for an Idealized Tropical Ocean Model

Throughout this paper, we have studied numerically the relative importance of current and thermocline–depth data for various wind stress errors. Since the wind stress error can vary in both zonal and meridional directions, the issue is not tractable analytically in the full model. To gain further insight, we study in this appendix an even simpler tropical ocean model. It results from considering the ocean only within a narrow equatorial band and neglecting the

contribution of meridional velocity, as well as using periodic boundaries instead of reflecting walls in the zonal direction.

This spatially one-dimensional model takes the nondimensional form

$$u_t + h_x = F - ru, \tag{A.1a}$$

$$h_t + u_x = -rh. \tag{A.1b}$$

It can be solved by expanding u, h, and F in Fourier series in x,

$$u(x, t) = (2\pi)^{1/2} \sum_{-\infty}^{\infty} \hat{u}(\xi, t) e^{i2\pi\xi x},$$

$$\hat{u}(\xi, t) = (2\pi)^{1/2} \int_0^1 e^{-i2\pi\xi x} u(x, t) dx,$$

where ξ is the zonal wavenumber. The solution can be written as

$$\begin{pmatrix} \hat{u}(\xi, t) \\ \hat{h}(\xi, t) \end{pmatrix} = A \begin{pmatrix} 1 \\ -1 \end{pmatrix} e^{-rt+i2\pi\xi t} + B \begin{pmatrix} 1 \\ 1 \end{pmatrix} e^{-rt-i2\pi\xi t} + \begin{pmatrix} \hat{u}_F(\xi) \\ \hat{h}_F(\xi) \end{pmatrix}, \tag{A.2}$$

where A and B are to be determined by the initial condition, and

$$\begin{pmatrix} \hat{u}_F(\xi) \\ \hat{h}_F(\xi) \end{pmatrix} = \frac{\hat{F}(\xi)}{r^2 + 4\pi^2\xi^2} \begin{pmatrix} r \\ -i2\pi\xi \end{pmatrix}. \tag{A.3}$$

The equilibrium velocity $\hat{u}_F$ and depth $\hat{h}_F$ are functions of the Rayleigh friction coefficient r, the wave number ξ, and the strength $\hat{F}(\xi)$ of the wind stress forcing.

This model contains only one type of wave, having the same speed of propagation both eastward and westward. Hence it does not capture the distinct contributions of Kelvin and Rossby waves, and of their reflections at the boundaries, to tropical data assimilation.

Since OI uses intermittent updating (Bengtsson et al. 1981), one type of observation is updated at all gridpoints for each case considered here. Let T be the updating interval; we have observations of $u(x, t)$ or $h(x, t)$ for $t = jT, j = 0, 1, 2, \cdots$; $\epsilon_u(x, t)$ and $\epsilon_h(x, t)$ denote the errors in the computed u and h at position x and time t. Notice that given complete observations of u (or h) at the updating times, ϵ_u (or ϵ_h) is reduced to zero, but not ϵ_h (or ϵ_u). After the updating time step, ϵ_h (or ϵ_u) will decrease, and ϵ_u (ϵ_h) may increase as a result of error redistribution due to the coupling in the system between u and h (Bube and Ghil 1981), and to wind stress errors. We also expand the errors in a Fourier series in x.

With perfect observations h (or u) at every gridpoint, the h (or u) field is corrected at each updating time, but the u (or h) field is not changed in univariate OI. After updating, the model starts from an initial state that has no error in the observed field, and does have errors in the other field. We study the error evolution in both fields between the first update and the next.

(i) First, we consider a case with errors in the initial state only and perfect wind stress. The true state is the model state in equilibrium with the wind stress, and the initial state is zero for both fields. This treatment follows closely that of Bube and Ghil (1981), who only dealt with initial-state error.

- Given h observations, one can show that

$$\hat{\epsilon}_u(\xi, T) = \rho(\xi, T)\hat{\epsilon}_u(\xi, 0) \tag{A.4a}$$

and

$$\rho(\xi, T) = e^{-rT} \cos(2\pi\xi T). \tag{A.4b}$$

Therefore, updating the h field reduces each Fourier coefficient of ϵ_u by a factor of $\rho(\xi, T) < 1$. The total error variance for each Fourier component before the next updating time step is given by

$$\hat{\epsilon}^2(\xi, T)|_h \equiv \hat{\epsilon}_u^2(\xi, T)|_h + \hat{\epsilon}_h^2(\xi, T)|_h = \hat{u}_F^2(\xi) e^{-2rT}. \tag{A.5}$$

The assimilation error is thus proportional to the initial error in the u field, and decays exponentially at the Rayleigh damping rate if there is no further updating.

- Given u observations, the total error variance for each Fourier component is, likewise,

$$\hat{\epsilon}^2(\xi, T)|_u = \hat{h}_F^2(\xi) e^{-2rT}. \tag{A.6}$$

The relative usefulness of h and u data depends on the ratio of initial errors in the other prognostic variable. Their usefulness is further related to the three parameters that determine the equilibrium state [cf. discussion of (A.3)]. With the Rayleigh friction coefficient value used here, h should be more useful, if the wind stress has zonal scale on the size of the Pacific or smaller; that is, $2\pi\xi \gg r$. The relationship between the zonal velocity u and the damping rate r can be seen from an extreme case: when $r = 0$, the equilibrium state is just an ocean at rest, with the depth variation along the equator governed by the wind stress.

(ii) Now, for the case of a systematic wind stress error, the true state is just zero for both h and u. The initial state is such that one field is completely corrected, and the other field is still in equilibrium with the wind stress. This case expands the results of Bube and Ghil (1981) from free to forced systems.

- When h data are available, the total error for each Fourier coefficient can be expressed as

$$\hat{\epsilon}(\xi, T)|_h = \frac{\hat{F}(\xi)}{r^2 + 4\pi^2\xi^2} \rho_1(\xi, T), \tag{A.7a}$$

where

$$\rho_1(\xi, T) = \left\{ r^2 + 4\pi^2\xi^2 \left[1 + e^{-2rT} - 2\cos(2\pi\xi T)e^{-rT} - \frac{r}{\pi\xi}\sin(2\pi\xi T)e^{-rT} \right] \right\}^{1/2} \Big/ (r^2 + 4\pi^2\xi^2). \quad \text{(A.7b)}$$

- With u data, we have

$$\hat{\epsilon}(\xi, T)|_u = \frac{\hat{F}(\xi)}{r^2 + 4\pi^2\xi^2}\,\rho_2(\xi, T), \quad \text{(A.8a)}$$

where

$$\rho_2(\xi, T) = \left\{ 4\pi^2\xi^2 + r^2 \left[1 + e^{-2rT} - 2\cos(2\pi\xi T)e^{-rT} - \frac{4\pi\xi}{r}\sin(2\pi\xi T)e^{-rT} \right] \right\}^{1/2} \Big/ (r^2 + 4\pi^2\xi^2). \quad \text{(A.8b)}$$

Note that for $T \to 0$, $\hat{\epsilon}|_u \to |\hat{h}_F|$, and $\hat{\epsilon}|_h \to |\hat{u}_F|$; that is, as updating becomes more and more frequent, there is a strong similarity between the systematic wind stress error case and the switch-on case.

For the values used here, $r \ll 2\pi\xi$ and $\rho_1(\xi, T)$ is smaller than $\rho_2(\xi, T)$, provided updating is relatively frequent, that is, roughly less than 40 days for wind stress errors with a zonal scale not exceeding the size of the Pacific basin. In this case, h data are more useful than u data for a systematic wind stress error (Fig. A1a). For a longer updating interval, u data are preferable. The point where the impact of u data exceeds that of h data depends on the wavenumber ξ: the higher the wavenumber of the erroneous wind stress, the shorter the updating intervals that make good use of u data (Fig. A1b). As the partitioning of initial errors between the h field and u field is proportional to $2\pi\xi/r$, the usefulness of the data depends on the error magnitude associated with the other data field, the same result that was obtained for the switch-on case.

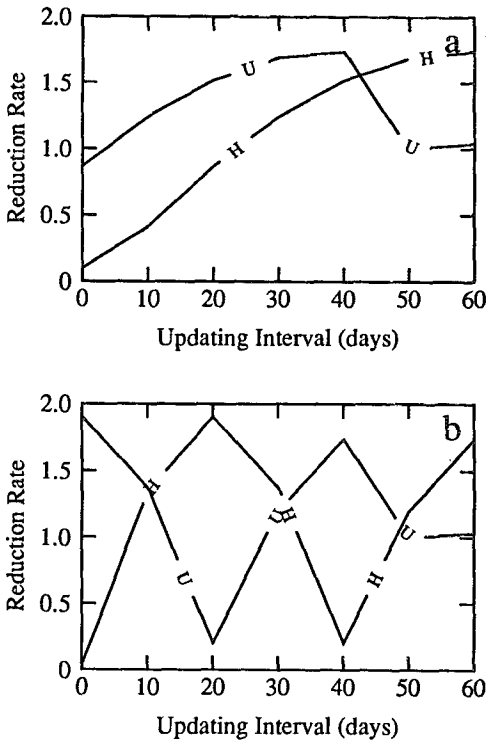

FIG. A1. Reduction rate (nondimensional) vs length of updating interval (in days) for the idealized model in the case of a constant wind stress error. (a) For the parameter values used in the numerical model: $\xi = \xi_0 = 0.0165$ and $r = 0.01$—i.e., wind stress error of basin size scale and damping time of 200 days. (b) For $\xi = 3\xi_0$ and same r. The reduction rate for updating with current or depth data only is denoted by the curve (-U-) or (-H-), respectively.

The reduction rate ρ in Eqs. (A.7) and (A.8) can be larger, however, rather than less than 1 for updating intervals that are too long (or too short). This possibly poor performance of the assimilation method is a major difference between the case of systematic wind stress error and of initial state error.

The exact values of the crossover point(s) between greater usefulness of the thermocline–depth and current data depends on the details of the model. It stands to reason that it should differ for the full numerical model, for which only $T = 30$ days was used, and the present, analytical model. The main point of this analysis is that the length of the updating interval in the data assimilation is an important ingredient in determining the ultimate usefulness of observing systems.

In numerical weather prediction, as data became more plentiful, operational centers changed from a 12-hour assimilation cycle to a 6-hour cycle. In seasonal-to-interannual prediction for the tropical ocean–atmosphere system, one can expect a similar shift from a one-month to a two-week cycle. It appears worthwhile to carry out an analysis similar to the one here, or corresponding numerical experiments, for a more complete model than the one in this appendix, having both Kelvin and Rossby waves and realistic boundary conditions. Such a study should help determine the effect of halving the update time on the relative usefulness of data from different sources.

REFERENCES

Anderson, D. L. T., and A. M. Moore, 1989: Initialization of equatorial waves in ocean models. *J. Phys. Oceanogr.*, **19**, 116–121.

Baer, F., 1977: Adjustment of initial conditions required to suppress gravity oscillations in nonlinear flows. *Beitr. Phys. Atmos.*, **50,** 350–366.

Bengtsson, L., M. Ghil, and E. Källén, Eds., 1981: *Dynamic Meteorology: Data Assimilation Methods.* Springer-Verlag, 330 pp.

Busalacchi, A. J., and J. J. O'Brien, 1981: Interannual variability of the equatorial Pacific in the 1960's. *J. Geophys. Res.*, **86,** 10 901–10 907.

Bube, K. P., and M. Ghil, 1981: Assimilation of asynoptic data and the initialization problem. *Dynamical Meteorology: Data Assimilation Methods,* L. Bengtsson, M. Ghil, and E. Källén, Eds., Springer-Verlag, 111–138.

Cane, M. A., and E. S. Sarachik, 1979: Forced baroclinic ocean motion. III. The linear equatorial basin case. *J. Mar. Res.*, **37,** 355–398.

——, and R. J. Patton, 1984: A numerical model for low-frequency equatorial dynamics. *J. Phys. Oceanogr.*, **14,** 1853–1863.

——, and S. E. Zebiak, 1985: A theory for El Niño and the Southern Oscillation. *Science,* **228,** 1085–1087.

Daley, R., 1981: Normal mode initialization. *Dynamical Meteorology: Data Assimilation Methods,* L. Bengtsson, M. Ghil, and E. Källén, Eds., Springer-Verlag, 77–109.

——, 1991: *Atmospheric Data Analysis.* University Press, 420 pp.

Gandin, L. S., 1963: *Objective Analysis of Meteorological Fields.* Gidrometeorologicheskoe Izdatel'stvo. [Translated by Israel Program for Scientific Translations, Jerusalem, 242 pp, 1965.]

Gelb, A., Ed., 1974: *Applied Optimal Estimation.* The MIT Press, 374 pp.

Ghil, M., 1989: Meteorological data assimilation for oceanographers. Part I: Description and theoretical framework. *Dyn. Atmos. Oceans,* **13,** 171–218.

——, and P. Malanotte-Rizzoli, 1991: Data assimilation in meteorology and oceanography. *Advances in Geophysics,* Vol. 33, Academic Press, 141–266.

——, S. E. Cohn, J. Tavantzis, K. Bube, and E. Isaacson, 1981: Applications of estimation theory to numerical weather predication. *Dynamical Meteorology: Data Assimilation Methods,* L. Bengtsson, M. Ghil, and E. Källén, Eds., Springer-Verlag, 77–109.

Hao, Z., 1991: Data assimilation and wind-stress error correction in a forced tropical ocean model. M. S. Thesis, Department of Atmospheric Sciences, University of California, Los Angeles, 57 pp. [Available from Z. Hao, Dept. of Atmospheric Sciences, UCLA, 405 Hilgard Ave., Los Angeles, CA 90024.]

Hayes, S. P., L. J. Mangum, J. Picaut, A. Sumi, and K. Takeuchi, 1991: TOGA-TAO: A moored array for real-time measurements in the tropical Pacific Ocean. *Bull. Amer. Meteor. Soc.,* **72,** 339–346.

Leetmaa, A., and M. Ji, 1989: Operational hindcasting of the tropical Pacific. *Dyn. Atmos. Oceans,* **13,** 465–490.

Lorenc, A. C., 1981: A global three-dimensional multivariate statistical interpolation scheme. *Mon. Wea. Rev.*, **109,** 701–721.

McPherson, R. D., K. H. Bergman, R. E. Kistler, G. E. Rasch, and D. S. Gordon, 1979: The NMC operational global data assimilation system. *Mon. Wea. Rev.*, **107,** 1445–1461.

Miller, R. N., 1990: Tropical data assimilation experiments with simulated data: The impact of the tropical ocean and global atmosphere thermal array for the ocean. *J. Geophys. Res.*, **95,** 11 461–11 483.

——, and M. A. Cane, 1989: A Kalman filter analysis of sea level height in the tropical Pacific. *J. Phys. Oceanogr.*, **19,** 773–790.

Moore, A. M., 1990: Linear equatorial wave mode initialization in a model of the tropical Pacific Ocean: An initialization scheme for tropical ocean models. *J. Phys. Oceanogr.*, **20,** 423–445.

——, and D. L. T. Anderson, 1989: The assimilation of XBT data into a layer model of the tropical Pacific Ocean. *Dyn. Atmos. Oceans,* **13,** 414–441.

——, N. S. Cooper, and D. L. T. Anderson, 1987: Data assimilation in models of the Indian Ocean. *J. Phys. Oceanogr.*, **17,** 1965–1977.

Périgaud, C., and P. Delecluse, 1989: Simulations of dynamic topography in the northwestern Indian Ocean with input of Seasat altimeter and scatterometer data. *Ocean–Air Interact.*, **1,** 289–309.

Philander, S. G., 1990: *El Niño, La Niña, and the Southern Oscillation.* Academic Press, 293 pp.

——, and R. C. Pacanowski, 1980: The generation of equatorial currents. *J. Geophys. Res.*, **85,** 1123–1136.

——, T. Yamagata, and R. C. Pacanowski, 1984: Unstable air–sea interactions in the tropics. *J. Atmos. Sci.*, **41,** 604–613.

——, D. Halpern, D. Hansen, R. Legeckis, L. Miller, C. Paul, R. Watts, R. Weisberg, and M. Winbush, 1985: Long waves in the equatorial Pacific Ocean. *Eos, Trans. Am. Geophys. Union,* **66,** 154.

——, W. J. Hurlin, and A. D. Siegel, 1987a: A model of the seasonal cycle of the tropical Pacific Ocean. *J. Phys. Oceanogr.*, **17,** 1986–2002.

——, W. J. Hurlin, and R. Pacanowski, 1987b: Initial conditions for a general circulation model of tropical oceans. *J. Phys. Oceanogr.*, **17,** 147–157.

Rutherford, I. D., 1972: Data assimilation by statistical interpolation of forecast error fields. *J. Atmos. Sci.*, **29,** 809–815.

Sheinbaum, J., and D. L. T. Anderson, 1990a: Variational assimilation of XBT data. Part I. *J. Phys. Oceanogr.*, **10,** 672–688.

——, and ——, 1990b: Variational assimilation of XBT data. Part II. Sensitivity studies and use of smoothing constraints. *J. Phys. Oceanogr.*, **10,** 689–704.

Smedstad, O. M., 1989: Data assimilation and parameter estimation in oceanographic models. Ph.D. thesis, The Florida State University, 124 pp. [Available from Geophysical Fluid Dynamics Institute, The Florida State University, Talahassee, FL 32306.]

Tziperman, E., and W. C. Thacker, 1989: An optimal-control/adjoint-equations approach to studying the oceanic general circulation. *J. Phys. Oceanogr.*, **19,** 1471–1485.

Zebiak, S. E., 1989: On the 30–60 day oscillation and the prediction of El Niño. *J. Climate,* **2,** 1381–1387.

Wunsch, C. I., 1988: Transient tracers as a problem in control theory. *J. Geophys. Res.*, **93,** 8099–8110.